World Conference on
Timber Engineering
Oslo 2023

STRUCTURAL PERFORMANCE OF REINFORCED GLULAM BEAMS

Laith I. Gharaibeh[1], Ghasan Doudak[2]

ABSTRACT: The performance of wood glulam beams is generally characterized by brittle behaviour with little to no post-peak strength. Attempts to enhance the post-peak behaviour of glulam beams have included principles of reinforcing the tension face, while promoting more ductile compression-side failure. In the current study, Near-Surface Mounted (NSM) rebars are utilized to reinforce glulam beams in order to enhance their performance when subjected to static and dynamic loading. The reinforcement rebars are installed inside grooves at the tension face of the beam, using epoxy adhesive. The reinforced glulam beams were tested statically in four-point bending and with simply supported boundary conditions. Another set of reinforced glulam beams was tested under simulated blast loads using a shock-tube device. Similar loading and boundary conditions were also applied during the dynamic tests. An analytical approach was developed, verified, and used to investigate glulam beams reinforced with steel, GFRP, and CFRP rebars. The result of this comparison indicated a significant enhancement in the maximum peak strength and stiffness of the reinforced beams using steel and CFRP rebars, while beams reinforced with GFRP rebar exhibited lower increases in strength and stiffness.

KEYWORDS: Reinforced Glulam, Steel reinforcement, NSM, Blast load, Shock-tube device.

1. INTRODUCTION

Glued laminated timber (Glulam) has been successfully used for decades in heavy timber construction, with recent examples including the Brock Commons building in B.C. Canada and the headquarters of the Swiss media corporation in Zurich, Switzerland. The behaviour of glulam in flexure is generally characterized as linear-elastic brittle, under both static and dynamic loading [1]. The ultimate flexural failure typically occurs on the tension face at a defect (e.g. knots) or in some instances at finger joints [2]. Several research studies have been conducted to enhance the post-peak performance of timber beams in order to produce a more ductile failure mode. Examples of these attempts include reinforcing the tension face of the beam in order to delay the development of cracks at the tension side. This also helped initiate crushing failure mode at the compression face which in turn facilitated the increase in the overall energy-dissipation capabilities of the beam elements. Lacroix and Doudak [3] reinforced glulam beams using fiber-reinforced polymers (FRP) and reported an increase of 20% to 40% in the moment capacity depending on the reinforcement configuration. Yang et al, [4] reinforced a series of glulam beam specimens by applying steel reinforcing rebars at the beam tension face using reinforcement ratios of 0.5%, 1%, and 1.7%. The study reported increases in the range of 32% to 45% in moment capacity. Kliger et al. [5] investigated a wide range of reinforcement ratios of steel and carbon fiber plates. The study found that a maximum reinforcement ratio of 2% was appropriate to avoid shear failure before the ultimate flexural capacity of the beam was reached. The study also reported an increase in moment capacity in the range of 57% to 96%, when compared to the reference unreinforced beam. The behaviour of structural elements under blast loading is also greatly affected by high strain rates, resulting from the short duration of the loading. Research in the field of blast effects on timber elements has generally focussed on individual components with idealized simply supported boundary conditions, including light-frame stud walls [6,7], glulam beams and columns [1], as well as cross-laminated timber (CLT) elements [8]. Although some attempts have been made to address timber-composite assemblies, these studies have been limited to FRP sheets [3], steel straps [9], and corrugated steel panels [10]. Different types of reinforcing materials can be used to strengthen glulam beams using rebars, such as steel, glass fiber-reinforced polymer (GFRP), and carbon fiber-reinforced polymer (CFRP). In addition to providing sufficient strength and stiffness, steel can also add a significant amount of ductility, which in turn enhances the structural response of the glulam elements under blast loading. In the current study, epoxy is used as a bonding agent as well as a coating material to protect the steel. One of the disadvantages of GFRP is its low stiffness, which reduces its efficiency as a reinforcement material. CFRP material has high stiffness,

[1] Laith I. Gharaibeh, University of Ottawa, Canada, Lghar082@uottawa.ca
[2] Ghasan Doudak, University of Ottawa, Canada, gdoudak@uottawa.ca

https://doi.org/10.52202/069179-0409

but it is also associated with a high cost. The current study aims to investigate possible retrofit techniques to reinforce glulam beams using the near-surface-mounting (NSM) method. The structural behaviour of reinforced glulam beams using steel, GFRP and CFRP rebars will also be examined analytically.

2. EXPERIMENTAL PROGRAM

2.1 METHODOLOGY

The overarching goal of the experimental program is to validate analytical approaches that would facilitate the analysis of composite timber-reinforcement elements using the NSM reinforcement method. The experimental program includes subjecting full-scale beam specimens to static and blast-simulated dynamic testing under similar loading configurations and boundary conditions. The NSM method involves hollowing out grooves in the perimeter of the beam, placing the reinforcements inside the grooves, and then applying the epoxy over the reinforcement and initiating the curing process. The installation process of the NSM rebar method is illustrated in Figure 1.

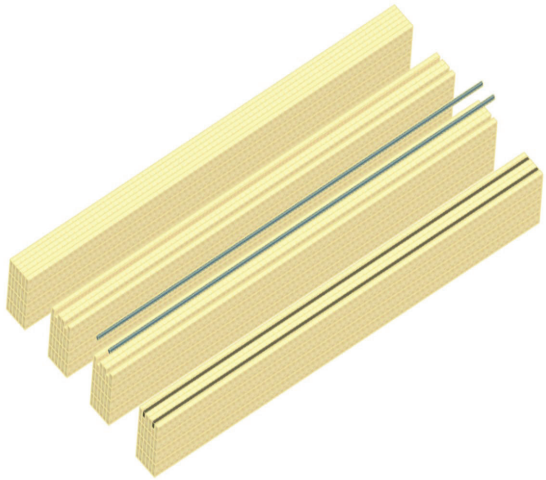

Figure 1: *NSM installation process*

The fact that the reinforcement is embedded inside the wood and surrounded by epoxy increases the contact surface area, unlike external reinforcement. Moreover, the reinforcement can be easily applied at the bottom or the side of the beam, unlike the external fabric reinforcements that have to be applied at both the bottom and side faces of the beam to provide suitable confinement and avoid debonding. The aesthetic appearance of the reinforcement could also be enhanced by adding a thin strip of wood to cover the groves after applying the reinforcement with the epoxy materials.

2.2 SPECIMENS AND TEST SETUP

Glulam beams with NSM reinforcement were tested statically and dynamically under a four-point bending. The procedure and configuration for the static and dynamic tests are presented in the following sections.

2.2.1 Static test

A set of glulam beams reinforced with 10M, 15M, and 20M steel rebars were tested statically. The beams consisted of a cross-sectional dimension of 137 mm x 191 mm and a length of 2.5 m. The beam grade was 24F-ES/NPG, produced by Nordic Structures. Wire gauge sensors were used to measure the displacement at the middle and one-third points of the beam span length. Strain gauges were also attached at the perimeter of the wood glulam section as well as along the steel reinforcements to measure the strain distributions. Furthermore, lateral supports were used at both ends of the beams to prevent out-of-plane buckling. The loads were applied to the beam specimens using a hydraulic jack, through an I-steel section. Load cells were placed at the supports to measure the reaction forces, as shown in Figures 2 and 3.

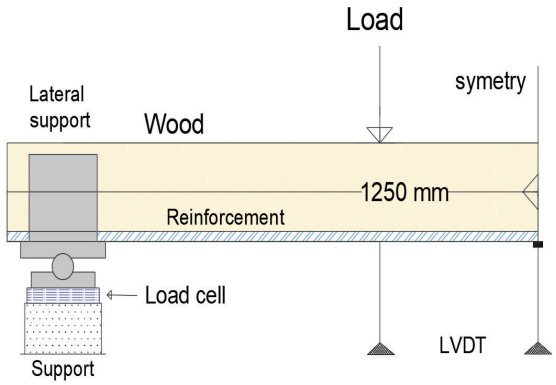

Figure 2: *Half-beam view for the static test.*

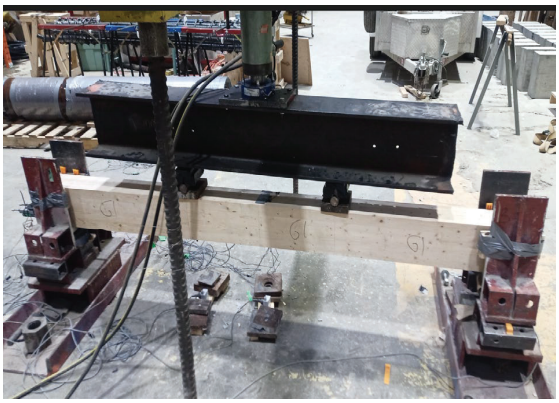

Figure 3: *Static test for glulam beam*

2.2.2 Dynamic test

A matched set of reinforced beams was tested under simulated blast loading using the shock-tube apparatus located at the University of Ottawa. Similar loading and boundary conditions to those described in the static loading tests were employed for the simulated blast tests, with the exception that the beam specimens were placed vertically, and the loads were applied horizontally. The shock-tube apparatus uses air pressure to create different

combinations of pressure and impulse to simulate the effect of far-field explosions. The device consists of three components: the driver, spool, and expansion sections. The driver section length can range from 305 mm to 5185 mm. Different combinations of pressures and impulses can be generated by changing the driver length. The shock-tube device is capable of generating a maximum pressure of 100 kPa and impulse of up to 2200 kPa-ms, as well as a positive phase duration of up to 70 ms. Aluminium foil layers are placed at the front and back of the spool, and when the desired air pressure in the spool is reached, the air pressure in the driver is drained, rupturing the aluminium foils and allowing the compressed air to propagate along the expansion section and interact with the test specimen. A load transfer device (LTD) mounted at the end-frame was used to collect the pressure and transfer it to the mounted specimen. The main components of the shock-tube device are shown in Figure 4.

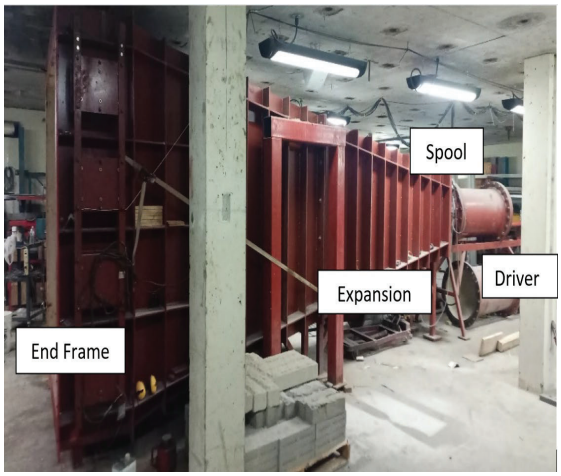

Figure 4: *Shock-tube device*

The displacement of the beam at mid-span was measured using linear variable displacement transducers (LVDTs) with the high-speed capability to capture the dynamic blast load. Dynamic load cells were used to measure the force reactions at the ends of the beams. The measurements were recorded using a data acquisition system (DAS) having a sampling rate of 10,000 samples per second. Furthermore, a high-speed camera having a recording rate of 2000 frames per second was used to capture the behaviour of the specimen and detect the failure mode during the test.

3. RESULTS AND DISCUSSION

3.1.1 Experimental Results

An example of the experiment results from the static test is presented in this section. The force-displacement curves for both the unreinforced and reinforced beams with 10M steel rebars are shown in Figure 5.

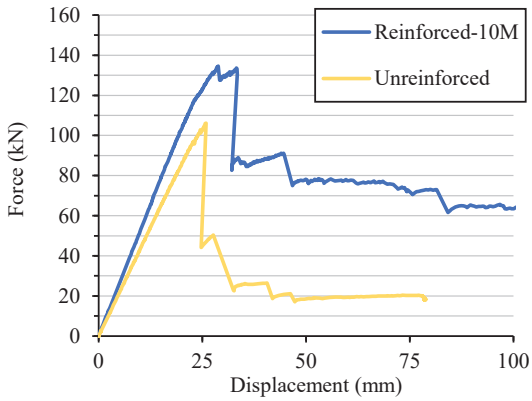

Figure 5: *Force-displacement curve*

From Figure 5 it can be observed that the strength and stiffness of the reinforced beam are significantly increased by the addition of the two steel reinforcement rebars. For this example, the strength and stiffness of the beam were increased by 34% and 23%, respectively, when compared to the unreinforced specimen. More importantly, it can be noted that the post-peak behaviour of the reinforced beam is greatly enhanced. A post-peak load carrying capacity in the range of 47% of the peak load is maintained until displacement levels are in excess of 100 mm.

Figure 6: *Damaged reinforced beam*

As shown in figure 7, cracks were developed and propagated at the tension face of the beam, and the epoxy material was fractured. The wood fibers at top of the beam were crushed due to compression stress. This type of failure mode is preferable since it enhances both the maximum peak strength as well as the post-peak behaviour of the glulam beam.

3.1.2 Analytical Results

The analysis approach used to predict the behaviour of the composite beam is the fiber section method. The analysis is conducted by setting an initial strain value at the top of the beam and selecting an initial position for the neutral axis depth (Z). Then, the strain profile along the depth of the beam is distributed linearly based on the Euler-Bernoulli beam theory by assuming that plane sections remain plane. The strain and stress are calculated at each

https://doi.org/10.52202/069179-0409

fiber based on the material model proposed by Buchanan [11], as shown in Figure 8.

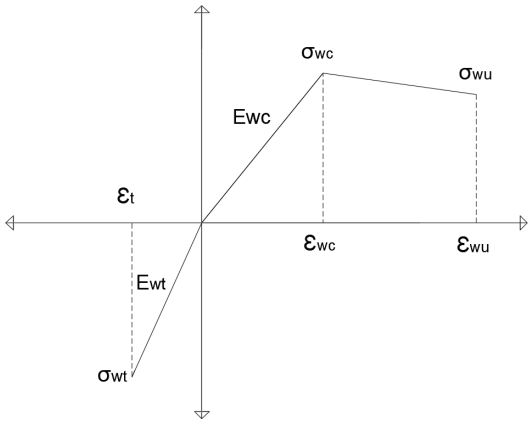

Figure 7: *Material wood model*

The model has been successfully used to simulate wood material behaviour in several previous studies [e.g., 1, 2]. In this model, σ_{wc} and σ_{wu} represents the maximum and ultimate stress in compression, respectively, and σ_{wt} is the maximum tensile stress. E_{wt} and E_{wc} are the modulus of elasticity for wood in tension and compression, respectively. ε_{wc} and ε_{wu} represent the strains at the maximum and ultimate stress in compression, respectively, while ε_{wt} is the failure strain at σ_{wt}. Following the calculation of the stresses at each fiber layer, the tension or compression force is calculated by taking the average stress at that fiber and multiplying it by the area of the fiber. The summation of the tension and compression forces from all fibers must satisfy equilibrium. If the equilibrium is not reached, a new value for depth Z is generated, and the entire procedure is repeated until the equilibrium is satisfied. The fiber moment is obtained by multiplying the force in the fiber by the distance to the neutral axis. The procedure is repeated for a new value of strain increment until the moment-curvature relationship for the beam section is achieved.

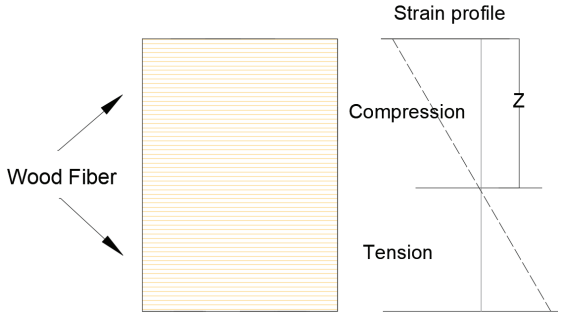

Figure 8: *Fiber section for glulam beam*

A VBA Excel-based code was developed and used to conduct the fiber section analysis and establish the stress-strain relationship along the depth of the beam. The effect of groove size was also considered in the analysis. Finally, the curvature is integrated twice to determine the displacement along the entire beam. The force-displacement curve obtained from this analytical procedure is compared with the experimentally obtained curve, as shown in Figure 10. The figure shows that the theoretical model provided a very good agreement with the experimental result in terms of force and displacement. Work is currently underway to extend the modeling capabilities beyond the peak load and to account for the behaviour of the reinforced beams.

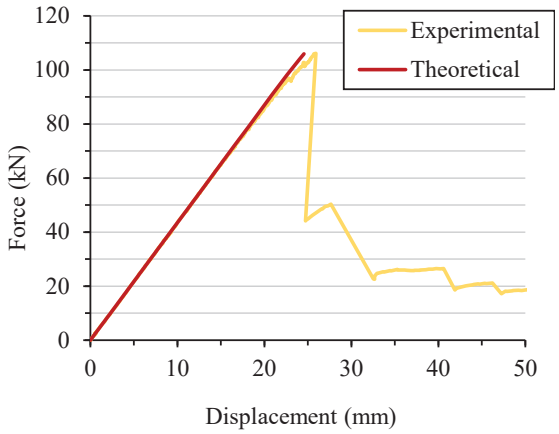

Figure 9: *Static test for glulam beam*

3.1.3 Reinforced beam

The analytical procedure presented in the previous section was used to compare the behaviour of glulam beams reinforced with steel, GFRP and CFRP rebars. For the steel rebar, an elastoplastic material model was used, as shown in Figure 11, where F_y represents the yield stress, E_s is the modulus of elasticity, and ε_y is the yielding strain. For the GFRP and CFRP materials, the stress-strain relationship is assumed to be linear, with E_g and E_c representing the modulus of elasticity, while F_g and F_c are the associated stresses, respectively. ε_c and ε_g are the failure strains for CFRP and GFRP materials, respectively, as shown in Figure 12.

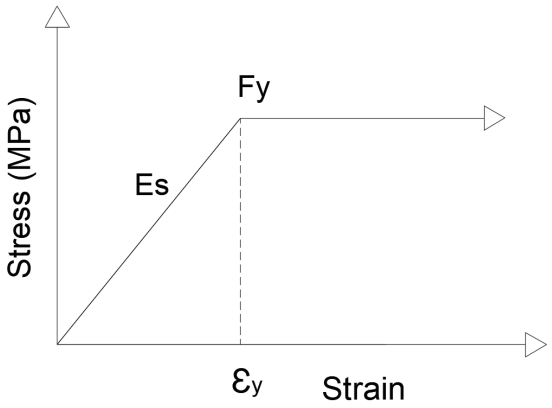

Figure 10: *Steel elastoplastic model*

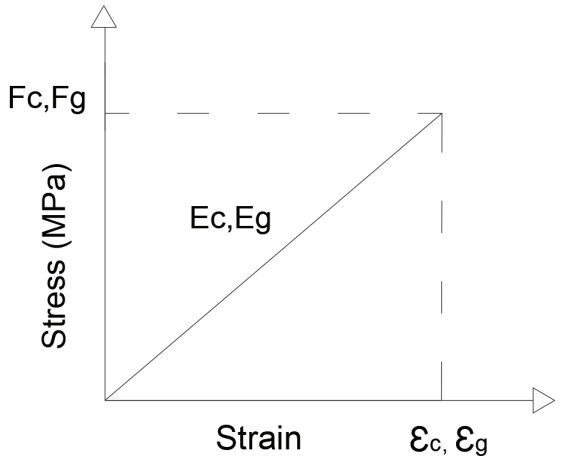

Figure 11: *GFRP and CFRP linear models*

For the reinforced beams, the forces at the reinforcements have to be included in the summation of the forces to satisfy the equilibrium along the cross-section. The reinforcements were assumed as concentrated elements since their cross-sectional area is very small compared to the glulam member. The analytical model was modified to accommodate the effect of the reinforcements in the sectional analysis. Figure 13 shows the wood fiber cross-section for the reinforced glulam beams, including the GRFP, CFRP, or steel rebar reinforcements.

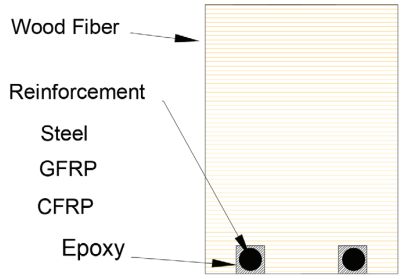

Figure 12: *Fiber-reinforced beam section*

For the purpose of the analytical comparison, US rebar sizes #4, #5 and #6 were used due to their availability in steel, GFRP and CFRP rebar sizes. The material property for the steel rebars was assumed to be according to ASTM 615 [12] with 420 MPa tensile strength and 200 GPa modulus of elasticity. The GFRP rebars were assumed to be consistent with those produced by MST Rebar Inc. in Canada [13], with 60 GPa in modulus of elasticity and 1,000 MPa minimum tensile strength, while the CFRP rebars were assumed to have 124 GPa modulus of elasticity and 2,000 MPa minimum tensile strength, similar to those produced by Hughes manufacturer in US, [14]. An example of a moment-curvature distribution along half the beam length is shown in Figure 14, for reinforced beams with #6 steel reinforcement rebars.

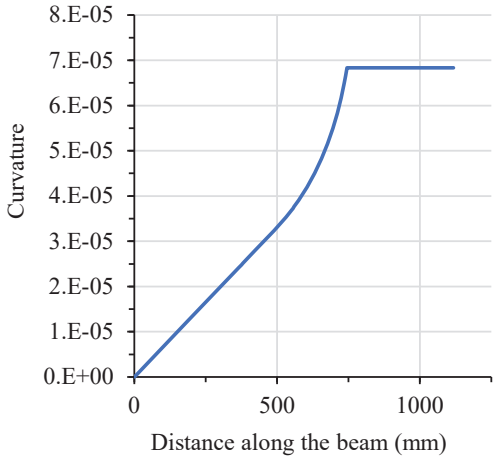

Figure 13: *Moment-curvature distribution*

Using the analytical model, the force-displacement curves obtained for the glulam beams reinforced with steel rebar sizes #4, #5 and #6 are compared, as shown in Figure 15.

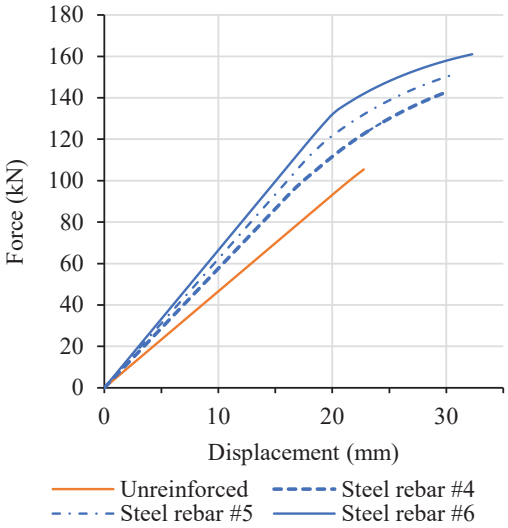

Figure 14: *Reinforced beam with steel rebar*

From this comparison, it can be observed that the strength of the reinforced glulam beams was increased by 35%, 45% and 53% when using rebar sizes #4, #5 and #6, respectively, compared to the unreinforced beam. The corresponding increases in stiffness was 24%, 34% and 53%, respectively. The curves using the GFRP reinforcement rebars are shown in Figure 16. It can be observed that the increase in strength is less than that observed in the beams analyzed with steel reinforcements, while for stiffness, only a minor increase is observed. The non-linear behaviour observed near the peak load in specimens with steel rebars is much less pronounced in GFRP rebars.

https://doi.org/10.52202/069179-0409

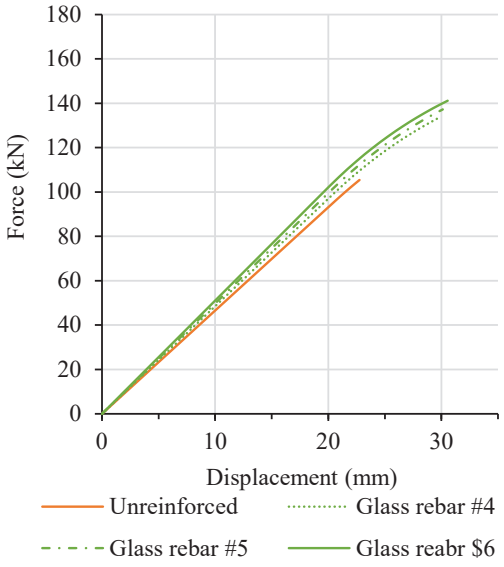

Figure 15: *Reinforced beam with GFRP*

Figure 17 presents the results for the beams with the CFRP reinforcement rebars, and shows increases in strength of 40%, 49% and 56%, using rebar sizes #4, #5 and #6, respectively, while the corresponding stiffness increases were 14%, 20% and 27%. The results show that the general increase magnitude is comparable to the steel rebars when it comes to the beam strength, however, the increase associated with stiffness is less, which can be attributed to the higher modulus of elasticity of the steel rebars.

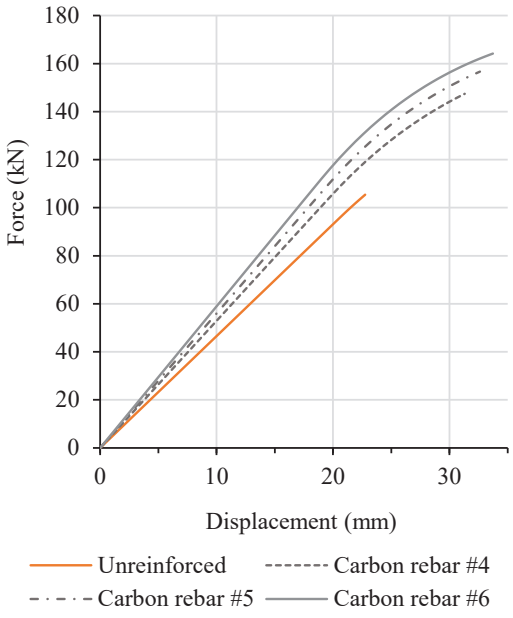

Figure 16: *Reinforced beam with CFRP*

A direct comparison between the three retrofitting options, illustrating the benefit of utilizing steel rebars, is shown in Figure 18 for the same rebar size (i.e., #6).

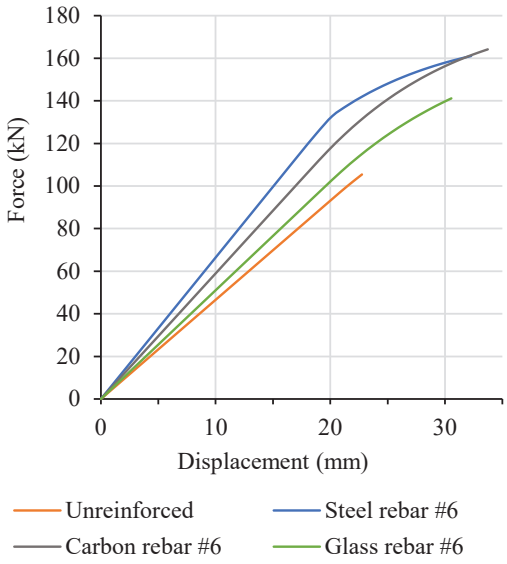

Figure 17: *Glulam beams with reinforcements*

4. CONCLUSIONS

Near-surface mounted rebars were used to enhance the performance of glulam beams, especially in the post-peak region. Reinforcements were embedded inside the beam at the tension face and adhered to the beam using epoxy. The behaviour of the reinforced beams was investigated experimentally, and results showed a significant enhancement in the strength, stiffness as well as post-peak behaviour. An analytical approach, developed based on the fiber method and using available wood constitutive models, was validated using the experimental results. The models were then used to compare the impact of using steel, GFRP and CFRP reinforcement rebars. The result of this comparison showed a significant enhancement in the maximum peak strength when using steel and CFRP rebars, while better enhancement in stiffness was obtained from the steel rebars. For beams reinforced with GFRP rebars, the increase in strength and stiffness was modest.

REFERENCES

[1] Lacroix, D. N., Doudak, G.: Effects of High Strain Rates on the Response of Glulam Beams and Columns. Journal of Structural Engineering, 144(5), 04018029, 2018.

[2] Lacroix, D. N., and Doudak, G. : Determining the Dynamic Increase Factor for Glued-Laminated Timber Beams" *Journal of Structural Engineering*, 144(9), 04018029, 2018.

[3] Lacroix, D.N., Doudak, G.: Experimental and Analytical Investigation of FRP Retrofitted Glued-Laminated Beams Subjected to Simulated Blast

Loading, Journal of Structural Engineering, 144(7), 04018089, 2018.
[4] Yang H., Liu W., Lu W., Zhu S., Geng Q: Flexural behavior of FRP and steel reinforced glulam beams: Experimental and theoretical evaluation. Constr. Build. Mater. 106:550–563, 2016.
[5] R. Kliger, M. Al-Emrani, M. Johansson, R. Crocetti, editors. Strengthening glulam beams with steel and composite plates, *Proceedings of the Asia-Pacific Conference on FRP in Structures,* 2007, Hong Kong.
[6] Lacroix, D., & Doudak, G. (2012). Behaviour of typical light-frame wood stud walls subjected blast loading. World Conference on Timber Engineering: Strength and Serviceability - Extreme Events. Auckland, New-Zealand.
[7] Lacroix, D. N., and Doudak, G. (2015). "Investigation of Dynamic Increase Factors in Light-Frame Wood Stud Walls Subjected to Out-of-Plane Blast Loading." *Journal of Structural Engineering*, 141(6), 04014159.
[8] Poulin, M. et al. (2017) Experimental and analytical investigation of cross-laminated timber panels subjected to out-of-plane blast loads: Journal of Structural Engineering: Vol 144, no 2,
[9] Lopez-Molina, A. and Doudak, G. (2019) "Retrofit techniques for cross-laminated timber (CLT) elements subjected to blast loads," *Engineering Structures*, 197, p. 109450.
[10] Lacroix, D.N., Doudak, G. and El-Domiaty, K. (2014) "Retrofit options for light-frame wood stud walls subjected to blast loading," *Journal of Structural Engineering*, 140(4).
[11]. Buchanan, A., H. (1990). "Bending strength of lumber." Journal of Structural Engineering, 116(5), 17.
[12] ASTM A615 / A615M-09, Standard Specification for Deformed and Plain Carbon-Steel Bars for Concrete Reinforcement, ASTM International, West Conshohocken, PA, 2009.
[13] MST-BAR® Manufactured by MST Rebar Inc., Toronto, Canada.
[14] Aslan™ 200 Carbon fiber reinforced polymer (CFRP) bars for structural strengthening, owens corning, 2018.

https://doi.org/10.52202/069179-0409